DNA-Templated Nickel Nanostructures and Protein Assemblies

ARTICLE *in* LANGMUIR · DECEMBER 2006

Impact Factor: 4.46 · DOI: 10.1021/la061740+ · Source: PubMed

Langmuir **2006,** *22,*

DNA-Templated Nickel Nanostructures and Protein Assemblies

Hector A. Becerril, Paul Ludtke, Barry M. Willardson, and Adam T. Woolley*

Department of Chemistry and Biochemistry, Brigham Young University, Provo, Utah, 84602

We report a straightforward method for the fabrication of DNA-templated nickel nanostructures on surfaces. These nickel nanomaterials have potential to be applied as nanowires, as templated catalyst lines, as nanoscale magnetic domains, or in directed protein localization. Indeed, we show here that histidine-tagged phosducin-like protein (His-PhLP) binds with high selectivity to both Ni^{2+}-treated surface DNA and DNA-templated nickel metal to create linear protein assemblies on surfaces. The association of His-PhLP with DNA-templated nickel ions or metal is reversible under appropriate rinsing conditions. Nanoscale DNA-templated protein assemblies might be useful in the construction of high-density protein lines for proteomic analysis, for example. Importantly, these nanofabrication procedures are not limited to linear DNA and can be applied readily to other self-assembled DNA topologies.

Introduction

DNA-templated nanofabrication is a powerful approach for producing nanostructures of various materials. DNA is a robust biopolymer that can withstand a range of pH, temperature, and solvation conditions. Chelating nitrogenated bases in the DNA molecule, as well as a polyanionic phosphate backbone, provide chemical handles[1] that make possible the fabrication of DNA-templated nanomaterials. Typically, sodium or other ions associated with nucleic acids are exchanged for higher-charge-density transition metal cations that can be reduced or further reacted to form DNA-templated solids. To date, this approach has been applied to make DNA-templated materials including metals such as silver,[2−4] platinum,[5] palladium,[6] gold,[7,8] cobalt,[9] and copper;[10−12] and semiconductors such as cadmium sulfide[13,14] and iron oxide.[15]

DNA templating that does not rely on cation exchange is also possible. For instance, DNA has been used as a scaffold for the localization of bifunctional molecules that serve as linkers between DNA and other nanostructures.[16] Examples of this strategy include the use of polycyclic aromatic amines[17] or long-chain positively charged surfactants[18] to direct the assembly of DNA and carbon nanotubes. Another approach[19] utilizes functionalized DNA oligonucleotides to assemble metal,[20] streptavidin,[12,21] or streptavidin-coupled nanostructures.[22] Finally, DNA molecules can be modified covalently to direct the assembly of specific cations[23] or organic molecules.[24]

Nickel nanostructures are of considerable interest because the electrical, magnetic, and catalytic properties of macroscale nickel-containing materials might also be valuable at the nanometer scale. In addition, nickel can serve as an intermediary in the assembly of histidine (His)-modified moieties. The His tag, a hexamer of the naturally occurring amino acid histidine, is utilized routinely in biochemical protocols as a molecular handle that mediates the reversible binding of labeled proteins to purification columns that contain nickel ions. Thus, it may be feasible for His-tagged proteins, as well as other His-labeled nanostructures, to be localized selectively and reversibly on nanoscale DNA-templated nickel.

Heterotrimeric GTP-binding proteins (G-proteins) are signal transducers that couple transmembrane receptors to their intracellular effectors. G-proteins are composed of Gα, Gβ, and Gγ subunits. Upon ligand-induced conformational changes in the receptor, bound GDP is exchanged for GTP on Gα, resulting in dissociation of GTP-bound Gα from the G$\beta\gamma$ complex. Phosducin-like protein (PhLP) is a widely expressed binding partner of G-protein $\beta\gamma$ subunit complexes and the cytosolic chaperonin containing TCP-1 (CCT). Recent findings show that PhLP is involved in the assembly of G$\beta\gamma$ dimer subunits and may act in concert with CCT in the G$\beta\gamma$ assembly process.[25]

Here we describe the surface fabrication of DNA-templated nickel nanostructures, which have not been reported previously. We also show the association of His-tagged PhLP (His-PhLP) with Ni^{2+}-treated surface DNA and DNA-templated nickel metal. We observe that His-PhLP binds selectively and reversibly to

* To whom correspondence should be addressed. Phone: 801-422-1701. Fax: 801-422-0153. E-mail: atw@byu.edu.

(1) Gu, Q.; Cheng, C.; Gonela, R.; Suryanarayanan, S.; Anabathula, S.; Dai, K.; Haynie, D. T. *Nanotechnology* **2006**, *17*, R14−R25.
(2) Braun, E.; Eichen, Y.; Sivan, U.; Ben-Yoseph, G. *Nature (London)* **1998**, *391*, 775−778.
(3) Keren, K.; Berman, R. S.; Braun, E. *Nano Lett.* **2004**, *4*, 323−326.
(4) Becerril, H. A.; Stoltenberg, R. M.; Monson, C. F.; Woolley, A. T. *J. Mater. Chem.* **2004**, *14*, 611−616.
(5) Ford, W. E.; Harnack, O.; Yasuda, A.; Wessels, J. M. *Adv. Mater.* **2001**, *13*, 1793−1797.
(6) Richter, J.; Mertig, M.; Pompe, W.; Mönch, I.; Schackert, H. K. *Appl. Phys. Lett.* **2001**, *78*, 536−538.
(7) Harnack, O.; Ford, W. E.; Yasuda, A.; Wessels, J. M. *Nano Lett.* **2002**, *2*, 919−923.
(8) Keren, K.; Kreuger, M.; Gilad, R.; Ben-Yoseph, G.; Sivan, U.; Braun, E. *Science* **2002**, *297*, 72−75.
(9) Gu, Q.; Cheng, C.; Haynie, D. T. *Nanotechnology* **2005**, *16*, 1358−1363.
(10) Monson, C. F.; Woolley, A. T. *Nano Lett.* **2003**, *3*, 359−363.
(11) Stoltenberg, R. M.; Woolley, A. T. *Biomed. Microdevices* **2004**, *6*, 105−111.
(12) Becerril, H. A.; Stoltenberg, R. M.; Wheeler, D. R.; Davis, R. C.; Harb, J. N.; Woolley, A. T. *J. Am. Chem. Soc.* **2005**, *127*, 2828−2829.
(13) Coffer, J. L.; Bigham, S. R.; Li, X.; Pinizzotto, R. F.; Rho, Y. G.; Pirtle, R. M.; Pirtle, I. L. *Appl. Phys. Lett.* **1996**, *69*, 3851−3853.
(14) Liang, H.; Angelini, T. E.; Braun, P. V.; Wong, G. C. L. *J. Am. Chem. Soc.* **2004**, *126*, 14157−14165.
(15) Nyamjav, D.; Ivanisevic, A. *Biomaterials* **2005**, *26*, 2749−2757.
(16) Ijiro, K.; Matsuo, Y.; Hashimoto, Y. *Mol. Cryst. Liq. Cryst.* **2006**, *445*, 207−211.
(17) Xin, H.; Woolley, A. T. *J. Am. Chem. Soc.* **2003**, *125*, 8710−8711.
(18) Xin, H.; Woolley, A. T. *Nanotechnology* **2005**, *16*, 2238−2241.
(19) Gothelf, K. V.; LaBean, T. H. *Org. Biomol. Chem.* **2005**, *3*, 4023−4037.
(20) Csáki, A.; Maubach, G.; Born, D.; Reichert, J.; Fritzsche, W. *Single Mol.* **2002**, *3*, 275−280.
(21) Niemeyer, C. M. *Trends Biotechnol.* **2002**, *20*, 395−401.
(22) Li, H.; Park, S. H.; Reif, J. H.; LaBean, T. H.; Yan, H. *J. Am. Chem. Soc.* **2004**, *126*, 418−419.
(23) Czlapinski, J. L.; Sheppard, T. L. *Bioconjugate Chem.* **2005**, *16*, 169−177.
(24) Gothelf, K. V.; Brown, R. S. *Chem.−Eur. J.* **2005**, *11*, 1062−1069.
(25) Lukov, G. L.; Hu, T.; McLaughlin, J. N.; Hamm, H. E.; Willardson, B. M. *EMBO J.* **2005**, *24*, 1965−1975.

DNA-templated nickel constructs to produce nanoscale linear protein assemblies. While other DNA-templated protein arrangements have been reported previously,[21,22,26] these approaches utilized biotinylated DNA sequences to direct the binding of streptavidin to periodically occurring, but discrete, locations on the DNA. Our methodology for nanofabricating DNA-templated protein assemblies is more general in the scope of proteins that can be deposited, requires no specially synthesized DNA, and yields high coverage of the DNA template with protein.

Experimental Section

Preparation of cDNA Constructs for PhLP and His-PhLP. Wild-type human PhLP with 3′c-myc and His_6 epitope tags was constructed in the bacterial expression vector pET15b (Novagen, San Diego, CA) as described by Lukov et al.[25] The wild-type human PhLP-TAP fusion construct was prepared by PCR amplification of human PhLP and the C-TAP tag from pZome-1-C vector (Cellzome, Cambridge, UK) followed by ligation and insertion into bacterial expression vector pETDUET-1 (Novagen). The integrity of both constructs was confirmed by sequence analysis.

Protein Expression and Purification. Wild-type human PhLP-myc-His in the pET15b vector was transformed in *Escherichia coli* DE3 cells by heat shock and was purified using nondenaturing Ni^{2+} chelate affinity chromatography.[27] Wild-type human PhLP-TAP in the pETDUET-1 vector was transformed in *E. coli* DE3 cells by heat shock and was extracted using BPER reagent (Pierce Biotechnology, Rockford, IL) followed by TAP tag purification as described by Rigaut et al.[28] The purified proteins were concentrated and exchanged into 20 mM HEPES, pH 7.2, 150 mM NaCl, 50% glycerol buffer. The concentration and purity of the proteins were determined as described by Lukov et al.,[25] with each protein exceeding 90% purity.

Substrate Preparation for Atomic Force Microscopy (AFM). We used both hydrophobic and hydrophilic silicon surfaces to align DNA and generate our nanomaterials. To prepare these substrates, we cleaned 1 cm^2 pieces of p-type [100] silicon wafers (TTI Silicon, Sunnyvale, CA) using piranha solution, rinsed them with purified water from an Easypure UV/UF system (Barnstead, Dubuque, IA), and dried the surfaces under a stream of nitrogen. Cleaned silicon squares were used directly as hydrophilic substrates. To produce hydrophobic surfaces, we dried the cleaned silicon pieces at 130 °C for 1 h and then exposed them to chlorodimethyloctadecylsilane (Aldrich, St. Louis, MO) vapor for 5 min. We removed the wafers from the oven and soaked them in acetone for 30 min followed by rinses with acetone, 2-propanol, and purified water.

In preparation for DNA alignment, we treated hydrophilic silicon squares with a 1 ppm aqueous solution of poly(L-lysine) (Ted Pella, Redding, CA) for 1 min followed by a purified water rinse; hydrophobic squares were used as prepared. We aligned λ DNA (New England Biolabs, Ipswich, MA) on both types of silicon substrates by translation[29] or wicking of a 1−4 μL droplet of a 1−5 ng/μL λ DNA solution in 10 mM Tris-HCl, 1 mM EDTA (both from Life Technologies, Grand Island, NY), pH 8.0 (TE buffer). Finally, we rinsed the aligned DNA substrates with purified water and dried them under a stream of nitrogen.

Both types of surfaces allowed the fabrication of nanostructures, but the hydrophilic silicon substrates were more susceptible to nonspecific deposition of His-PhLP when rinsing was not optimal. We attribute this behavior to electrostatic interactions between the positively charged His tag and the negatively charged silicon dioxide surface.

Substrate Preparation for Scanning Transmission Electron Microscopy (STEM). We took copper grids coated with an unsupported carbon film (Ted Pella) and treated them with a 4 μL droplet of a 5 ng/μL λ DNA solution in TE buffer for 5 min or until evaporation was complete. We then rinsed the substrates with purified water. This procedure deposited the DNA strands on the carbon surface without subjecting it to large mechanical forces that could fracture the carbon film. We found that translation of the solution to align DNA fragments on the carbon surface was unsuccessful because of the fragile nature of the unsupported carbon membranes.

Preparation of DNA−Ni^{2+} Complexes and DNA-Templated Nickel Metal. We prepared saturated ethanolic solutions of $NiCl_2$ (Acros Organics, Geel, Belgium) or $Ni(NO_3)_2$ (Baker & Adamson, Easton, PA) by dissolving 50 mg of either salt in 500 μL of ethanol, vigorously stirring for 10 min, and centrifuging at 14 000 rpm for 5 min. We observed no effects of the nickel salt anions on the nanostructures we fabricated.

To produce Ni^{2+}-treated DNA, we exposed surface-aligned DNA substrates to the ethanolic nickel ion solution for 5 min in an environment saturated with ethanol vapor, after which we rinsed abundantly with ethanol and dried the substrate under a stream of nitrogen.

To make DNA-templated nickel metal, we prepared a reducing solution, dissolving 4 mg of $NaBH_4$ (EMD, Gibbstown, NJ) in a mixture of 100 μL of concentrated NH_4OH and 900 μL of purified water, stirring for 5 min, and allowing the solution to sit overnight before use. We treated aligned DNA substrates with 15 μL of the saturated ethanolic nickel solution for 5 min in an enclosed chamber, added 200 μL of the reducing solution, and allowed the reaction to proceed for 5 min. Finally, the substrates were rinsed with purified water and dried under a stream of nitrogen.

Preparation of DNA−Nickel−Protein Nanocomposites. We prepared a protein dilution buffer, containing 20 mM HEPES, (Mallinckrodt Baker, Phillipsburg, NJ) pH 7.2 and 150 mM NaCl (Columbus Chemical Industries, Columbus, WI). We also prepared a nickel binding equilibration buffer, containing 20 mM Tris-HCl, pH 8.0, 500 mM NaCl, and 50 mM imidazole (Acros Organics). We prepared a solution containing 70 ng/μL His-PhLP in a 1:1 mixture of the dilution and equilibration buffers and used it within 1 h. We incubated substrates, having either Ni^{2+}-treated DNA or DNA-templated nickel metal, with 10 μL of the His-PhLP solution for 1 min, rinsed abundantly with purified water and dried under a gentle nitrogen stream. For control experiments, a 70 ng/μL solution of PhLP lacking the His-tag was used to treat the same type of substrates in a similar way.

AFM. We collected tapping mode height images with a Multimode IIIa AFM (Veeco, Sunnyvale, CA) using microfabricated, aluminum-coated silicon cantilever tips (Nanoscience Instruments, Phoenix, AZ). We used an active isolation system (MOD1-M, Halcyonics, Göttingen, Germany) to reduce vibrational noise. Our imaging parameters were tip resonance frequency, 50−70 kHz; free oscillation amplitude, 0.9−1.1 V; amplitude setpoint, 0.5−0.8 V; and scan rate, 0.4−1.4 Hz. We processed our images offline to remove background curvature.

STEM. We recorded STEM images on a Tecnai 20 FEI instrument, with a 200 kV acceleration potential and a 3.4 kV extraction voltage. We used the cross-correlation method of the Tecnai software to correct for sample drift during nanometer-resolved energy-dispersive X-ray (EDX) analysis.

Results and Discussion

Figure 1 displays tapping mode AFM height data of unmodified surface-aligned λ DNA, immobilized DNA that has been ion exchanged with Ni^{2+}, and DNA-templated nickel metal. The height of DNA increases by almost a factor of 2 after incubation with a saturated ethanolic solution of Ni^{2+} followed by ethanol rinsing (Figure 1B). This increase in DNA height persists until the substrate is rinsed with an aqueous solution, which returns the DNA height to its unmodified value. Figure 1C shows a linear DNA-templated nickel metal nanostructure on a silicon surface, fabricated as outlined in the Experimental Section. The morphology of these metal nanostructures, as revealed by AFM,

(26) Yan, H.; Park, S. H.; Finkelstein, G.; Reif, J. H.; LaBean, T. H. *Science* **2003**, *301*, 1882−1884.
(27) Savage, J. R.; McLaughlin, J. N.; Skiba, N. P.; Hamm, H. E.; Willardson, B. M. *J. Biol. Chem.* **2000**, *275*, 30399−30407.
(28) Rigaut, G.; Shevchenko, A.; Rutz, B.; Wilm, M.; Mann, M.; Séraphin, B. *Nat. Biotechnol.* **1999**, *17*, 1030−1032.
(29) Woolley, A. T.; Kelly, R. T. *Nano Lett.* **2001**, *1*, 345−348.

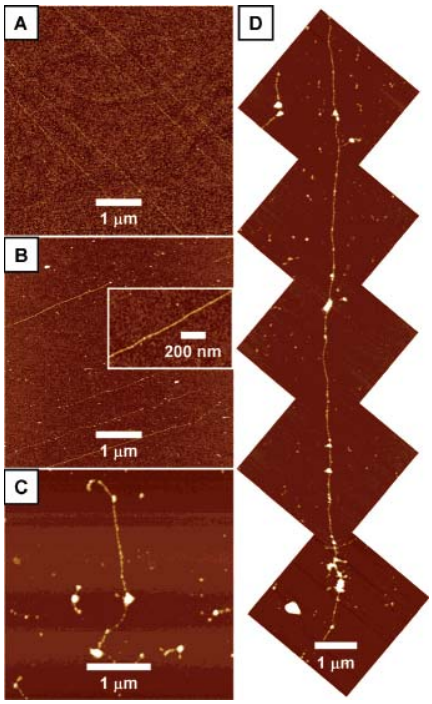

Figure 1. Tapping mode AFM height images of the synthesis of DNA-templated nickel. (A) Surface-aligned λ DNA molecules; *Z* scale is 3 nm. (B) DNA treated with Ni^{2+} and rinsed with ethanol; *Z* scale is 10 nm. (C−D) Linear nickel metal nanostructures made from surface DNA; *Z* scale is 50 nm in (C) and 100 nm in (D).

is that of a chain of closely spaced nickel nanoparticles, with ∼12 nm cross-sectional dimensions. Figure 1D shows a completely extended λ DNA molecule that is covered continuously with such nickel nanoparticles. This image demonstrates that our method for fabrication of nickel nanostructures does not cleave or otherwise damage the DNA template, allowing long DNA molecules to be plated with nickel, without loss of their structural integrity. Importantly, linear or two-dimensional assemblies of DNA-templated nickel nanoparticles could form ordered nanoscale magnetic storage units[9] or serve as catalytic seeds for the nanoscale patterned growth of materials such as carbon nanotubes.[30,31]

We used analytical electron microscopy to further characterize these DNA-templated nickel structures. Figure 2A and B shows STEM images of two separate DNA-templated nickel nanostructures grown on carbon-coated copper grids. Due to the hydrophobic nature of these surfaces, the DNA strands tend to bundle or entangle when deposited on such substrates, producing nonlinear nickel nanostructures. We observe a granular but quasicontinuous assembly of nickel nanoparticles along the DNA template. The average width of the observed features in the thinner, unbundled regions is ∼17 nm, which agrees well with the measured AFM height of ∼12 nm. Due to the finely focused electron beam in STEM, it is possible to selectively probe well-defined, nanometer-sized regions in the sample under study. Figure 2C shows an EDX spectrum obtained from a region in the nickel nanostructure in Figure 2B. The spectrum shows prominent nickel L_α and K_α peaks at 0.851 and 7.477 keV, respectively. Less intense carbon, oxygen, and silicon peaks from surface adsorption are observed, as well as copper and cobalt

(30) Geng, J.; Li, H.; Golovko, V. B.; Shephard, D. S.; Jefferson, D. A.; Johnson, B. F. G.; Hofmann, S.; Kleinsorge, B.; Robertson, J.; Ducati, C. *J. Phys. Chem. B.* **2004**, *108*, 18446−18450.

(31) Shi, J.; Lu, Y. F.; Tan, K. F.; Wang, X. W. *J. Appl. Phys.* **2006**, *99*, 024312.

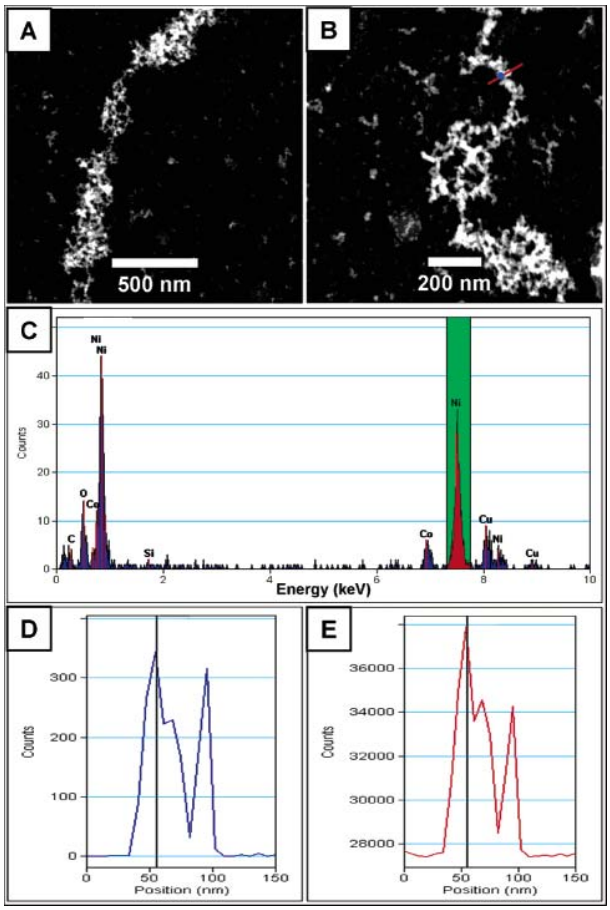

Figure 2. STEM images and nanometer-resolved composition analysis of DNA-templated nickel metal nanostructures. (A−B) STEM images of DNA-templated nickel nanostructures. (C) EDX spectrum obtained from the location indicated by the blue dot in (B). (D) Integration of characteristic nickel X-ray peaks (green region in C) from EDX spectra collected at 5 nm intervals along the red line in (B). (E) Total signal profile at the high-angle annular dark-field detector along the same red line.

peaks from the supporting grid and the pole piece of the electromagnetic objective lens, respectively. We profiled the composition of the nanostructure in Figure 2B by taking a series of EDX spectra at 5 nm intervals along the red line. We integrated the signal from the nickel K_α peak in each spectrum to obtain a cross section (Figure 2D) and compared this profile with that generated from the signal collected at the high-angle annular dark-field detector (Figure 2E). The two plots have nearly identical shapes, indicating that the analyzed nanostructure is mainly composed of nickel.

We also studied the interaction of PhLP and His-PhLP with our DNA-templated nickel assemblies. Figure 3A shows an AFM height image of individual PhLP molecules on a surface; their average height is 4.2 nm with a standard deviation of 1.1 nm. The PhLP dimensions agree remarkably well with the 4.8 nm average diameter determined from the crystallographic structure of the closely related protein, Phosducin (PDB 2TRC).[32] Further, we observed no difference in the AFM heights of PhLP and His-PhLP. Figure 3B depicts a control substrate showing that unmodified DNA does not interact with PhLP under the conditions utilized in our experiments. In another control, unmodified surface DNA and His-PhLP display little specific interaction after incubation and rinsing treatments (Figure 3C). Figure 3D depicts

(32) Gaudet, R.; Bohm, A.; Sigler, P. B. *Cell* **1996**, *87*, 577−588.

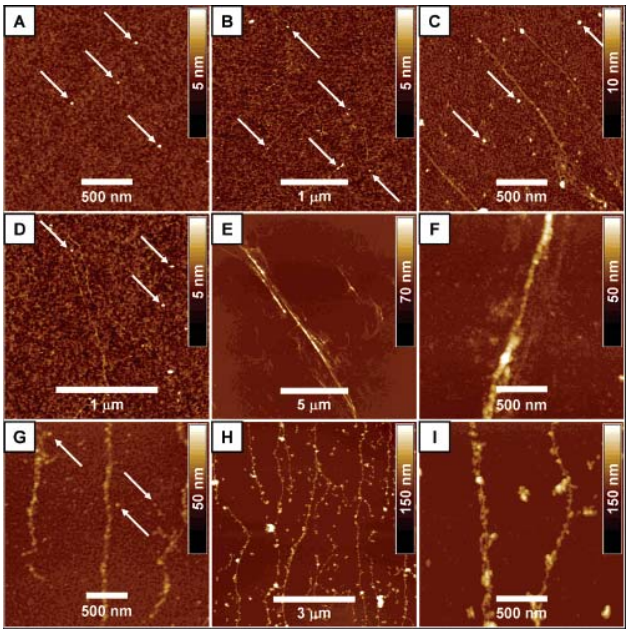

Figure 3. AFM height images of DNA-templated nickel−protein nanocomposites. (A) PhLP on silicon dioxide. (B) DNA incubated with PhLP. (C) DNA incubated with His-PhLP. (D) DNA treated with Ni^{2+}, rinsed with ethanol, and exposed to PhLP. (E−F) DNA treated with Ni^{2+}, rinsed with ethanol, and exposed to His-PhLP. (G) DNA-templated nickel metal nanostructures exposed to PhLP. (H−I) DNA-templated nickel metal nanostructures exposed to His-PhLP. All substrates were rinsed with purified water after protein treatment. Individual protein molecules are indicated with white arrows in (A−D, G).

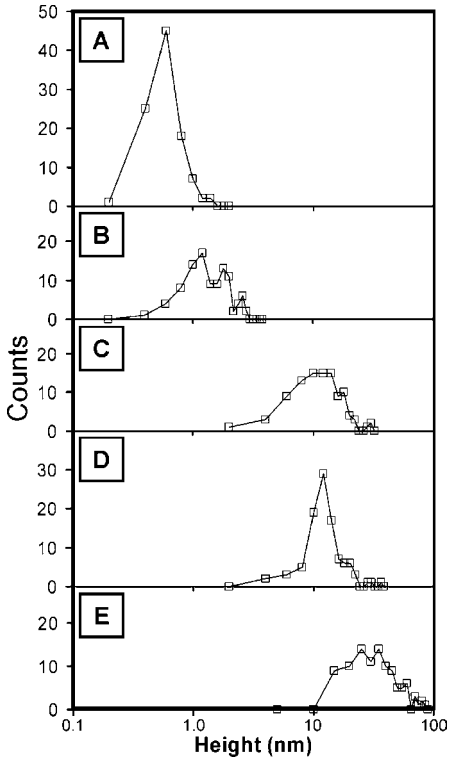

Figure 4. Evolution of the AFM height distribution of DNA-templated materials. (A) Surface-aligned λ DNA. (B) DNA complexed with Ni^{2+}. (C) DNA complexed with Ni^{2+} and treated with His-PhLP. (D) DNA-templated nickel metal. (E) DNA-templated nickel metal treated with His-PhLP. Mean heights are 0.5, 1.4, 12, 12, and 35 nm in (A−E), respectively, and RSDs range from 40% to 47%.

the effect of incubation of PhLP with Ni^{2+}-treated surface DNA; not only do the DNA and the protein remain separated but also the DNA height reverts to that of untreated DNA, an indication that the imidazole buffer may deplete exposed Ni^{2+} cations from the DNA. In contrast, when we incubated Ni^{2+}-treated surface DNA with His-PhLP, a dramatic ∼10 nm height increase was observed on all DNA features (Figure 3E and F). The selectivity of the His-PhLP for the DNA template was high, as surrounding regions were free from nonspecific protein deposition. We found that some His-PhLP deposited in the vicinity of the surface DNA, resulting in broadened AFM features relative to the original DNA. The less-than-sharp edges on these protein lines are probably due to the diffusion of Ni^{2+} from the DNA to nearby surface regions during incubation with protein; His-PhLP molecules also bind in these diffused Ni^{2+} regions.

Figure 3G shows several DNA-templated nickel metal lines that have been incubated with PhLP. Some free protein molecules are present on the surface, but the height and overall appearance of the nickel metal nanostructures are unchanged (see Figure 1C and D). On the other hand, when DNA-templated nickel metal is incubated with His-PhLP, we observe a significant, >20 nm height increase for the surface lines, as well as a change in morphology (Figure 3H and I). In addition, the background substrate is essentially free of nonspecific deposition of His-PhLP, and the edges of the DNA-templated nickel-His-PhLP composites are sharper than those in Figure 3E and F. These observations can be explained by a protein localization process in which the His-PhLP selectively attacks high-energy sites along the DNA-templated nickel metal, where nickel atoms are more available for reaction. This selective attack and chelation process does not, during the short duration of the treatment, generate an excess of nickel cations that diffuse from the DNA-templated metal to neighboring areas. Thus, protein deposition along the metal nanostructure is not totally uniform, and a protein-free background is obtained.

Figure 4 summarizes the distributions of AFM heights for the DNA-templated nickel and protein features we made. The effects of supplying surface DNA with Ni^{2+}, reducing to nickel metal, and adding His-PhLP are evident. Interestingly, we observe that Ni^{2+}-treated surface DNA exposed to His-PhLP undergoes a height increase that corresponds to ∼2 layers of protein, while DNA-templated nickel metal appears to accommodate up to ∼5 layers of His-PhLP. We believe that because the His-PhLP binding sites on the Ni^{2+}-treated surface DNA are abundant, closely spaced, mobile, and generally accessible, a smoothing effect is exerted that prevents locally high concentrations of His-PhLP. In contrast, for DNA-templated nickel metal, the number, accessibility, and mobility of the His-PhLP binding sites are controlled by crystallographic factors; thus, favorable facets on nickel nanoparticles may react more abundantly with His-PhLP and increase local coverage.

Finally, we have investigated conditions that allow the straightforward removal of His-PhLP from DNA-templated nickel metal. We took DNA-templated nickel metal−His-PhLP composites, incubated them with different Ni^{2+} solutions, and rinsed with purified water for 3 min. The results are summarized in Table 1; two controls (the unmodified DNA-templated nickel metal and the nickel metal−His-PhLP composite) are included for ease of comparison. We observe that His-PhLP largely remains localized on the DNA-templated nickel metal after a 15 min treatment with ethanolic Ni^{2+} and is not removed completely even after a 1 h exposure to this solution. Interestingly, this result suggests that surfaces with multiple types of proteins might

Table 1. Height of DNA-Templated Nickel−His-PhLP Nanostructures upon Incubation with Different Solutions

treatment conditions	mean AFM height (nm)	% RSD
control 1. DNA-templated nickel metal	12	40
control 2. DNA−nickel−protein nanocomposite	35	47
ethanolic Ni^{2+} (saturated, ∼0.4 M), 15 min	32	61
aqueous Ni^{2+} (0.6 M), 15 min	19	58
ethanolic Ni^{2+} (saturated, ∼0.4 M), 60 min	18	31
aqueous Ni^{2+} (0.6 M), 60 min	12	38

be obtained through a multistep procedure wherein new DNA is aligned on a substrate and treated with ethanolic Ni^{2+} after the formation of other DNA-templated nickel metal−His-protein composites. In contrast, we determined that treatment with aqueous Ni^{2+} completely removes the His-PhLP from the DNA-templated nickel, possibly by offering more abundant and favorable chelating sites for the His tag in an environment that can solvate the protein. Importantly, aqueous Ni^{2+} solutions for His-tagged protein removal can dislodge the protein without damaging the underlying nickel nanostructures. On the other hand, when we utilized 0.5 M imidazole buffer, rapid removal of the His-PhLP was observed in conjunction with etching of the nickel metal, which would limit the reusability of the DNA-templated nanostructures.

In conclusion, we have reported the fabrication of DNA-templated nickel metal nanostructures that could find applications as patterned lines of catalytic, magnetic, or protein domains. We have also demonstrated that both surface DNA treated with Ni^{2+} and DNA-templated nickel metal reversibly bind His-PhLP. On the basis of our results from the His-PhLP model system, we expect other His-tagged proteins and nanostructures to be localizable on DNA-templated nickel. This development is an important addition to the existing repertoire of DNA-templated interactions and enables the DNA-directed self-assembly of His-tagged materials. From a biochemical vantage point, our findings could be useful in the fabrication of very high-density protein assemblies that could enhance the study of protein−protein and protein−substrate interactions. For instance, it should be feasible to use AFM to probe whether G-protein $\beta\gamma$ subunits bind to our Ni−His-PhLP composites, which would confirm the potential for evaluating protein−protein interactions in this system. Importantly, our methodology does not require access to cleanroom equipment or to other lithographic techniques to achieve fine patterning, although our procedures are compatible with standard microfabrication methods. Indeed, the combination of our approach with top-down microscale patterning could prove advantageous in the development of applications for DNA-templated nickel and protein nanomaterials.

Acknowledgment. We thank Dr. Richard R. VanFleet and Dr. Jeff Farrer of the BYU Electron Microscopy Laboratory for initial training on the STEM. This work was supported in part by the Army Research Laboratory and the U.S. Army Research Office under Grant No. DAAD19-02-1-0353. Héctor A. Becerril thanks the BYU Chemistry and Biochemistry Department for support from the Charles E. and Margaret P. Maw Graduate Research Fellowship.

LA061740+